(2) If self-induced filters were formed, the drainage performance was significantly affected by the geotextile being initially dry.
(3) If the backfill material does not contain fine particles, self-induced filters were not formed behind the geotextile.
(4) In order to examine the composition of soil and geotextile without disturbing the sample structure, the block sampling method by *in situ* freezing was found effective. Further, it was difficult to directly observe the mechanism of self-induced filters by using a scanning electron microscope because the mechanism is likely to be changed by the drying process.

The test reported was performed using specific soils and geotextiles, so further investigation is needed to generalize the results. It was reconfirmed, however, that tests need to be performed under realistic *in situ* conditions in order to estimate meaningful drainage performance.

REFERENCES

1. Haliburton, T. A. and Wood, P. D., Evaluation of the US army corps of engineers gradient ratio test for geotextile performance. *Second Int. Conf. Geotextiles* (1982).
2. Hoare, D. I., Synthetic fabrics as soil filters: a review. *ASCE* (1982) GT10.

Geotextiles and Geomembranes 4 (1986) 241–268

A Reinforcing Method for Steep Clay Slopes using a Non-woven Geotextile

F. Tatsuoka and H. Yamauchi

Institute of Industrial Science, University of Tokyo, Roppongi, Minato-ku, Tokyo, Japan

ABSTRACT

The effect of non-woven geotextile reinforcement on the stability and deformation of two clay test embankments is examined based on their performance for about 3 years for the first embankment and about 1½ years for the other. Horizontal planar sheets of a non-woven geotextile are expected to work in three ways: for compaction control; for drainage; for tensile reinforcement. The degree of stability of the steep slopes of the test embankments decreased during heavy rainfall. It is found that the use of non-woven geotextile reinforcement may effectively improve embankment performance. Only the stability analysis in terms of effective stresses can explain the performance of the test embankments. The horizontal creep deformation of the embankments during 2–3 years, which is partly attributed to the creep deformation of the non-woven geotextile, was found to be small. The results of both laboratory bearing capacity tests of a strip footing on a model sand ground reinforced with the non-woven geotextile and plane strain compression tests on sand specimens reinforced with the non-woven geotextile show that the non-woven geotextile gives tensile reinforcement to soils.

NOTATION

c'	cohesion intersect of soil in effective stress
E	Young's modulus
K_p	$(1 + \sin\phi')/(1 - \sin\phi')$
u_w	pore water pressure

Geotextiles and Geomembranes 0266-1144/86/$03·50

R	rate of reinforcing
$(R_T)_i$	rupture strength per unit width of a geotextile sheet in the ith layer.
SF	safety factor
T	total tensile force in geotextiles sheets per unit width of an embankment
$(T_A)_i$	pull-out resistance per unit width of a geotextile sheet in the ith layer
α	tensile force per unit width of a geotextile
γ_t	total unit of soil
ϵ	strain
ν	Poisson's ratio
σ	total stress
σ'	effective stress
τ	shear stress
τ_f	shear strength of soil
ϕ'	angle of internal friction of soil in effective stress
ϕ_μ	friction angle between soil and a geotextile

1 INTRODUCTION

In spite of its high tensile stiffness the use of steel reinforcement is restricted to selected cohesionless soils to avoid a serious reduction in the effective stress on its surface caused by the increase in pore water pressure. Although polymer geogrid is more effective than steel reinforcement for tensile reinforcement of cohesive soils,[1] this material, like steel, lacks any drainage ability. The ideal reinforcement for nearly saturated cohesive soils is therefore a low-cost stiff material with an ability to drain the soil. Since such a material is currently not available, a method to reinforce medium to low height (say less than 7 m) clay embankments by means of a non-woven geotextile has been investigated by constructing two test embankments (Fig. 1). Their post-construction performance has been partly reported elsewhere.[2]

The first test embankment (embankment I) was constructed in June 1982 and was demolished in October 1985. The second one (embankment II) was constructed in March 1984 and about 70 m^3 of water was supplied from a pond made on the crest during 2 weeks in October 1985 to critically evaluate its stability. The observation of the performance of the embankment has continued. The embankments were made using a kind of volcanic ash clay which is locally called Kanto loam (see Table 1). This kind of soil has a high natural water content of the order of 120–130% and a high

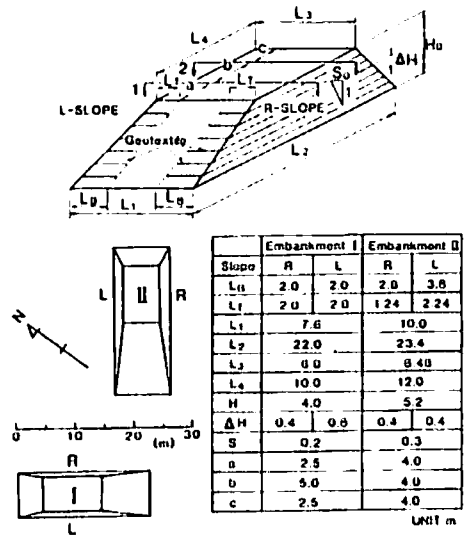

	Embankment I		Embankment II	
Slope	R	L	R	L
L_0	2.0	2.0	2.0	3.6
L_1	2.0	2.0	1.24	2.24
L_2	7.6		10.0	
L_3	22.0		23.4	
L_4	0.0		8.48	
H	10.0		12.0	
ΔH	4.0		5.2	
S	0.4	0.6	0.4	0.4
a	0.2		0.3	
b	2.5		4.0	
c	5.0		4.0	
	2.5		4.0	

UNIT m

Fig. 1. Initial dimensions of two test embankments constructed at Chiba Experiment Station, Institute of Industrial Science, University of Tokyo.[2]

degree of saturation of the order of 80% and is characterized by its high sensitivity of 4–5. Although the intact soil has a rather large shear strength due to its natural cementation, this soil becomes considerably weakened by remolding. Thus many rather steep-sided embankments constructed with this volcanic ash clay experienced large deformation, or failure, during filling or during heavy rainfall or earthquakes. Since a very large area in Japan is covered with various kinds of volcanic ash clays, there is a need for a method to construct stable side slopes using these materials.

The test embankments have steep slopes, being 1 : 0·2 (vertical to horizontal) for embankment I and 1 : 0·3 for embankment II. These slopes were reinforced with horizontal planar sheets of a non-woven geotextile (Fig. 2). The non-woven geotextile was used for three purposes: for allowing better compaction of the fill; for draining water quickly out of the embankment to prevent an increase in pore water pressure during heavy rainfall; for tensile reinforcement of embankments. In this paper, the experience obtained by continuous observation for about 2–3 years of these two instrumented test embankments is described together with the results of stability analyses. Also, results are given for laboratory plane strain compression tests and small model tests on reinforced soils.

TABLE 1
Properties of Soil

Intact ground	*Embankment I*
	at filling (June 1982)
w_n (%) ≒ 120	w (%) ≒ 100
ρ_d (g/cm^3) ≒ 0·52	at demolishing (Oct. 1985)
w_L (%) = 168	w (%) ≒ 93[d]
w_P (%) = 115	S_r (%) ≒85[d]
PI = 53	ρ_d (g/cm^3)≒ 0·69[d]
D_{50} = 14·5 μm	q_c (kN/m^2) = (4–6) × 10^2
clay content (<5 μm) = 29%	*Embankment II*
silt content (5–74 μm) = 63%	at filling (Oct. 1985)
sand content (>74 μm) = 8%	w (%) ≒ 120
TC[a] ϕ' = 29·6°	S_r (%) ≒ 90
TC[a] c' (kN/m^2) = 6·8	ρ_d (g/cm^3) ≒ 0·55–0·65
TE[b] ϕ' = 31·2°	q_c (kN/m^2) = (0·5–1) × 10^3
TE[b] c' (kN/m^2) = 8·9	for mechanically compacted layers or
q_c[c] (kN/m^2) = (1–3) × 10^3	= (2–7) × 10^2
	for manually compacted layers about 1 m next to the shoulder

[a]$\overline{CU}$ triaxial compression test.
[b]$\overline{CU}$ triaxial extension test.
[c]Cone penetration resistance.
[d]Averaged excluding near the crest.

2 CONSTRUCTION METHOD

Soil excavated from nearby intact ground of Kanto loam was used as the fill material. Each soil layer was compacted to a 40 cm thickness using compaction plant except within about 1 m of the face where manual compaction was used. A spun-bonded (needle-punched) 100% polypropylene non-woven geotextile was used (Table 2). The mechanical and hydraulic properties of the geotextile are reported elsewhere.[2] Tensile tests were performed on the geotextile at a strain rate of 1%/min by means of a newly developed tensile testing device (Fig. 3) where a test piece of geotextile can be confined by pressures under plane strain conditions (no change in the width of the test piece). The effects of both pressure confinement[3] and plane strain restraint were found important for the non-woven geotextile. Details of the tensile tests will be presented in a subsequent paper.

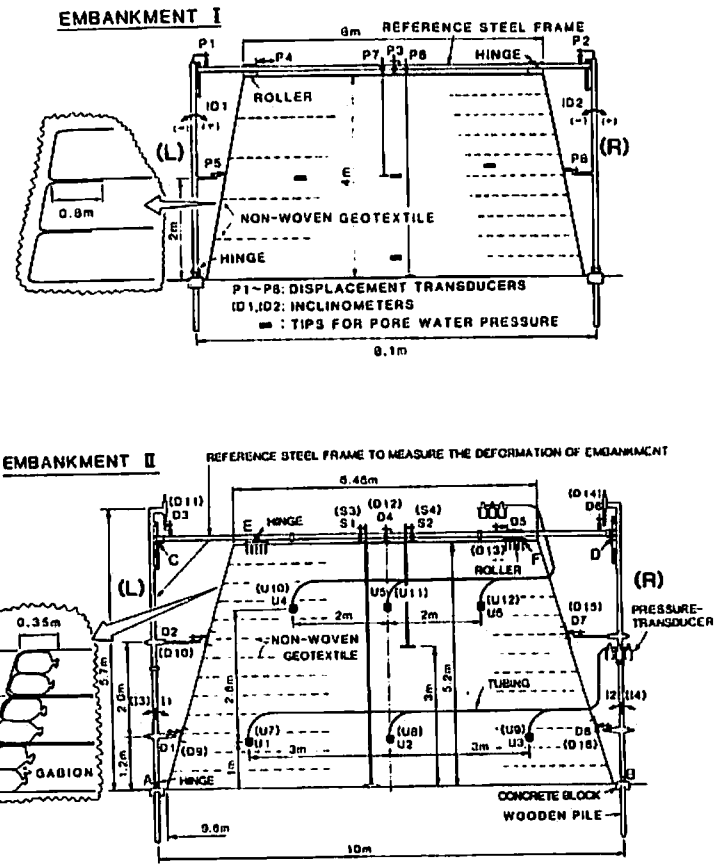

Fig. 2. Cross-sections of test embankments.[2]

TABLE 2
Mechanical and Hydraulic Properties of Non-woven Geotextile

Fiber density, ρ_f (g/cm^3) = 0·31
Fiber diameter, d_f (μm) = 0·40
Mass per unit area, μ (g/m^2) ≒ 400
Unstressed thickness (mm) = 3–4
Permeability in plane (cm/s)[a] ≒ 2×10^{-1} to 3×10^{-2}
Friction angle at interface with Kanto loam under water (degrees)[a] = 28–37[c]
Force per unit width at 15% elongation, $\alpha_{0\cdot15}$ (kN/m)[b] = $4{\cdot}26 + 0{\cdot}006\,75\sigma_0$
Force per unit width at peak, α_f (kN/m)[b] = $14{\cdot}7 + 0{\cdot}017\sigma_0$
Poisson's ratio, ν_g[d] = 0·0

[a]For normal stress, σ_0 (kN/m^2) = 0–313·6.
[b]For normal stress, σ_0 (kN/m^2) = 0–196.
[c]These values are similar to the angle of internal friction at large strains of Kanto loam.
[d]The value when compressed in the direction normal to the plane.

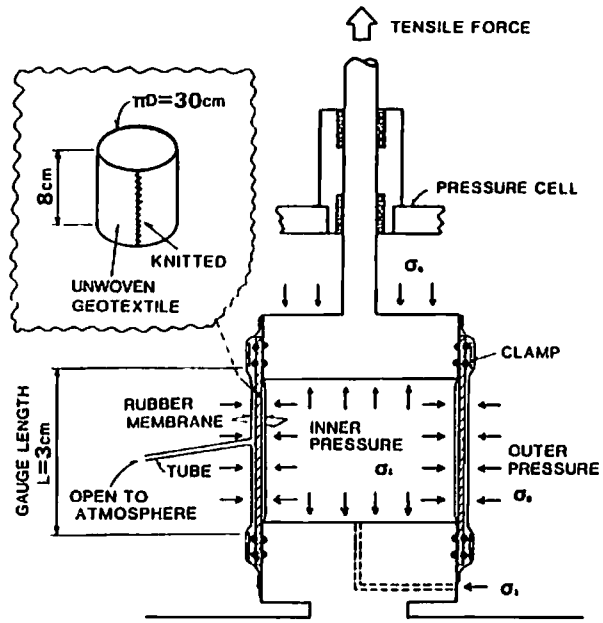

Fig. 3. Tensile testing apparatus (in plane strain tests; the inner pressure σ_i is controlled so that the circumferential length of the test piece is constant during test).

When compressed in a direction normal to its plane the non-woven geotextile exhibits a zero Poisson's ratio (ν_g). This provides a significant advantage in the tensile reinforcement of soils since the non-woven geotextile is extended in the horizontal (axial) direction only when the horizontal (axial) tensile force is applied. As shown later, it was found from laboratory tests that the non-woven geotextile can act much more effectively as tensile soil reinforcement than rubber sheets having a similar tensile stiffness but a Poisson's ratio of 0·49.

As shown in Fig. 2, the vertical spacing of the geotextile reinforcement was too large (80 cm) for the left-hand side slope of embankment I and the length was too small for the right-hand side slope of embankment II as compared to the values to be used in practice. These dimensions were selected to make the stability of the slopes critical so that the slopes would experience large deformation, and even failure, during heavy rainfall.

For embankment I, the flat slope faces were made and they were wrapped around with geotextile round the soil at the face (Fig. 2(a)). This method of face construction was found to be time-consuming and the confinement of the soil next to the slope face is lost when the soil is compressed vertically. Therefore, for embankment II two layers of gabions made of the non-woven geotextile and filled with Kanto loam were placed at each previous layer of the slope before placing the soil layer and the gabions were wrapped with the geotextile (Fig. 2(b)). The gabions were well compressed vertically when placed so that they will not be compressed by further filling and loading. It was found that the gabions help the compaction near the slope surfaces and also prevent a local failure in the soil adjacent to the slope face during heavy rainfall. No structural facing elements were used. To avoid ultraviolet light deterioration of the geotextile exposed at the slope surfaces, some measures would be needed when using this reinforcing method in actual construction projects.

3 BEHAVIOUR OF TEST EMBANKMENTS

Figure 4 shows the variation of displacements, pore-water pressures and rainfall with time for embankment II between April 1984 and October 1985. The measuring method is described elsewhere.[2] The antecedent precipitation index (API) at time t is defined as

$$\text{API} = P_0 + KP_1 + K^2P_2 + \ldots + K^nP_n \tag{1}$$

in which K is a constant less than 1·0, P_0 is the rainfall for one day preceding the time t concerned and P_n is the daily rainfall on the nth day

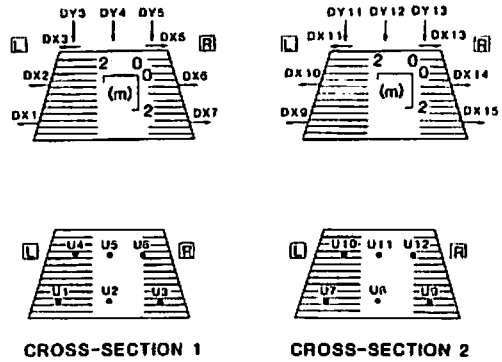

Fig. 4. Performance of embankment II between May 1984 and October 1985.

before time t. The API represents the humidity condition; it was found that when a value for K of 0·8 is used the variation of the API with time corresponds well to that of the pore-water pressures. Generally, when the API became higher than around 50 mm, the pore-water pressures in the test embankment increased, resulting in increased deformation of the embankment. It can also be seen that the behaviour of the embankment at the two measuring cross-sections is very similar. Figure 5 shows the detailed records for 4 days in June 1984 when the embankment experienced the largest rate of deformation.

From these results and similar results for embankment I the following points emerge.

(1) It can be seen from Figs 4–6 that the settlement is generally much larger than the outward horizontal displacement of slope which is a good indicator of the degree of instability of such steep slopes. A similar deformation was observed for the right-hand slope of embankment I (Figs 7 and 8). Since the major part of the settlement was due to one-dimensional compression of the soil, this kind of settlement would have occurred even if the slopes had been retained by means of very stable massive walls. Furthermore, it may also be seen from Fig. 6 that for embankment II the total outward horizontal displacement of the left-hand slope reinforced with longer sheets of geotextile is as small as 1·2–1·8 cm at the crest, which is smaller than that for the right-hand slope reinforced with shorter sheets of geotextile. The left-hand slope of embankment I experienced a large displacement due to a large local compression in the lowest soil layer, probably due to too large a vertical spacing of geotextile

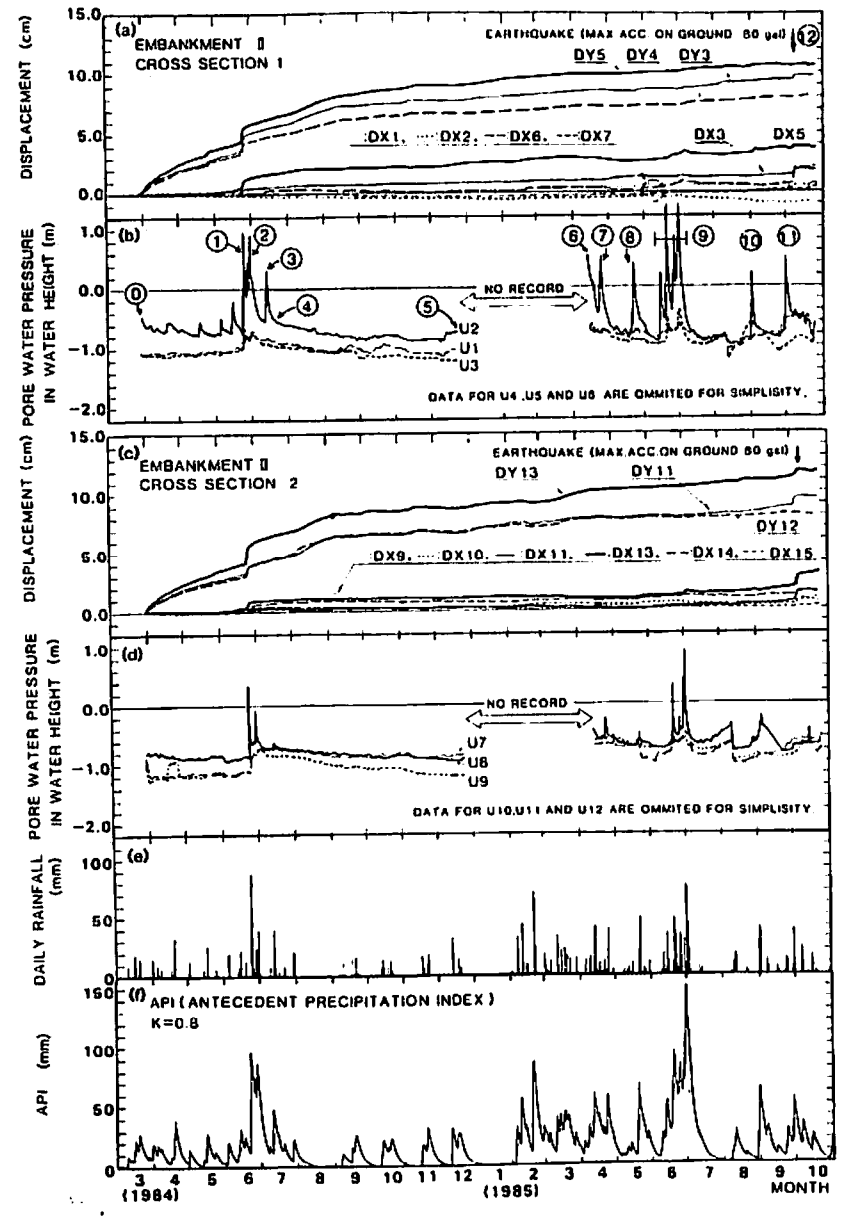

Fig. 4. —*contd.*

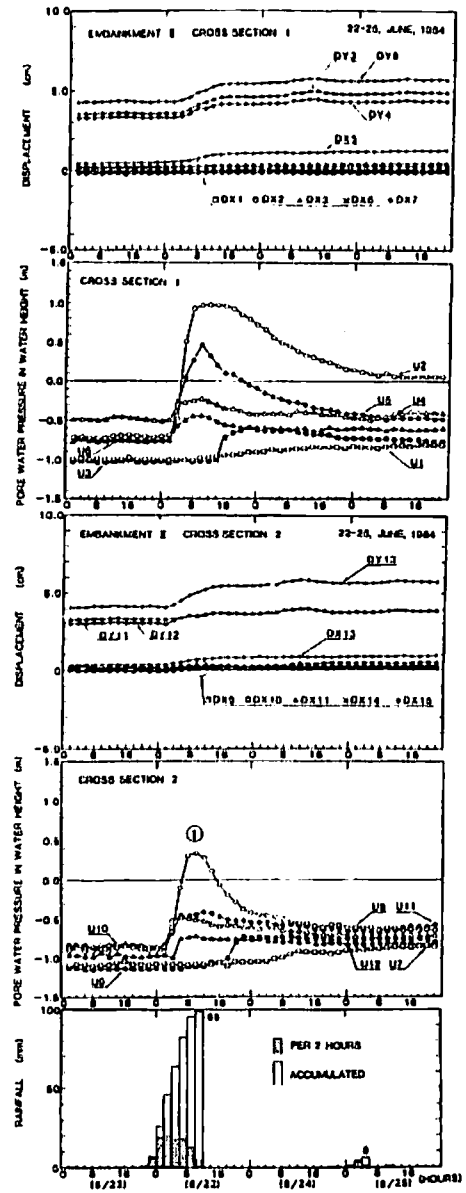

Fig. 5. Detailed record for 4 days in June 1984; embankment II.

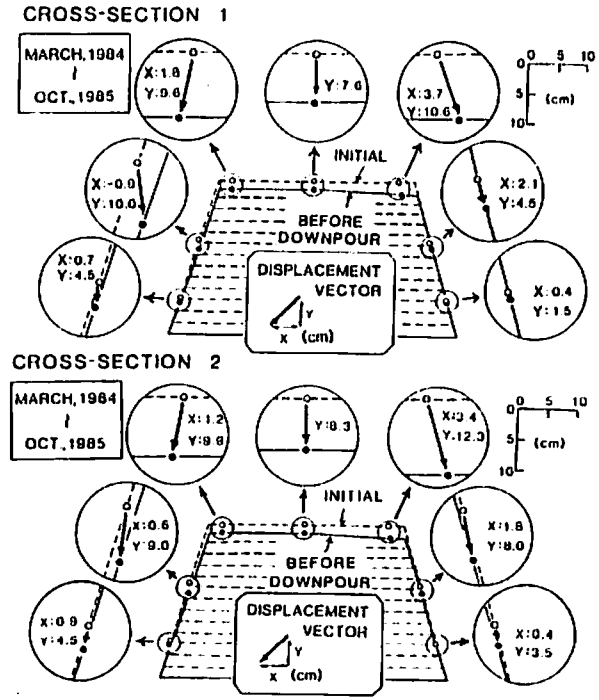

Fig. 6. Total displacements at representative points between May 1984 and October 1985; embankment II.

sheets. Therefore it seems that sufficiently long non-woven geotextile sheets with a not too large vertical spacing can effectively reinforce such clay steep slopes.

(2) The crest of embankment II settled in proportion to the accumulated rainfall in the first year (1984), whereas the settlement increased at a very much lower rate in the second year (Fig. 9(a)). It seems that this kind of settlement can be attributed to the collapse of the soil by wetting. For embankment II the outward horizontal movement in the first year is much larger than in the second year. The outward horizontal movement increased with increase in the accumulated rainfall in the first year (Fig. 9(b)). Similar behaviour was also observed for embankment I. Therefore it is clear that most of the deformation of the embankments was associated with rainfall.

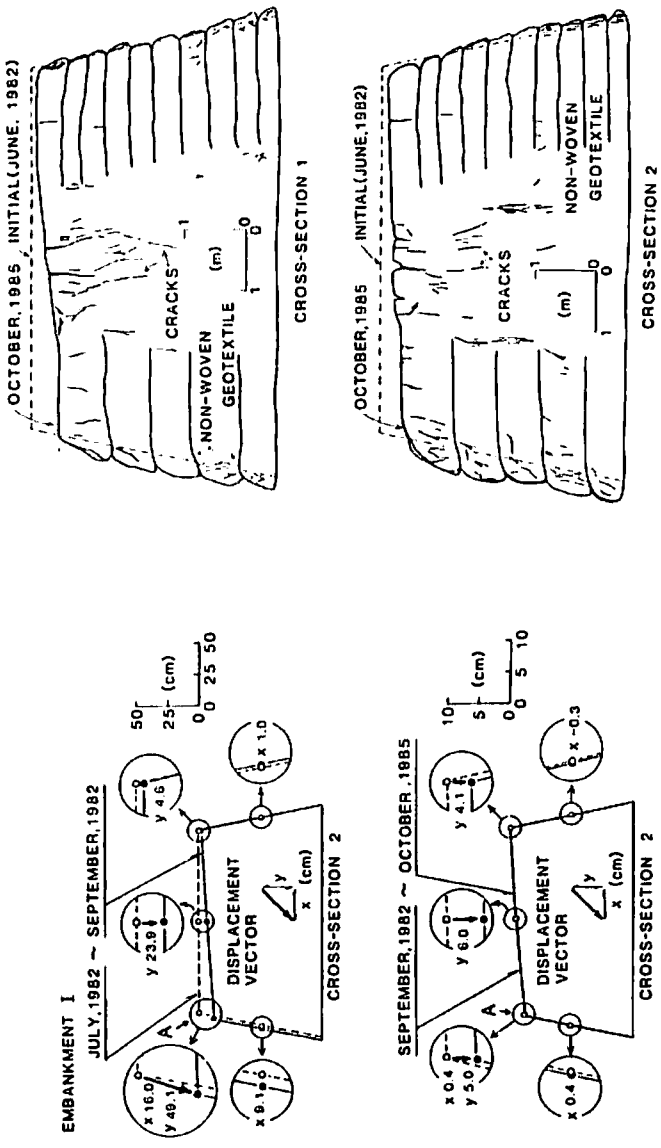

Fig. 8. Exposed cross-sections of embankment I (October 1985).

Fig. 7. Total displacements at representative points between 13 July 1982 and 16 September 1982 and between 16 September 1982 and 18 October 1985; cross-section 2 of embankment I (displacements in two directions were measured only at the point A).

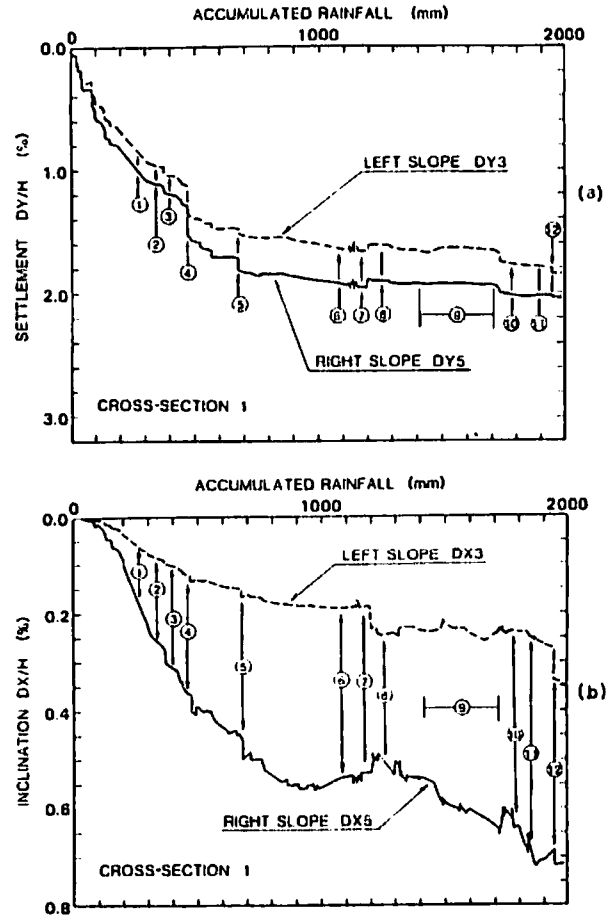

Fig. 9. Typical relationships (a) between settlement and accumulated rainfall and (b) between inclination of slope and accumulated rainfall; embankment II (see Fig. 4(b) for the legend of the numbers in circles).

(3) It may be seen in Fig. 4 that for embankment II, when the API is lower than about 50 mm, the negative pore-water pressure or suction did not decrease from its equilibrium value of about −1·0 m head of water. During the first year the outward horizontal displacement increased at a relatively large rate only when the negative value of pore-water pressures

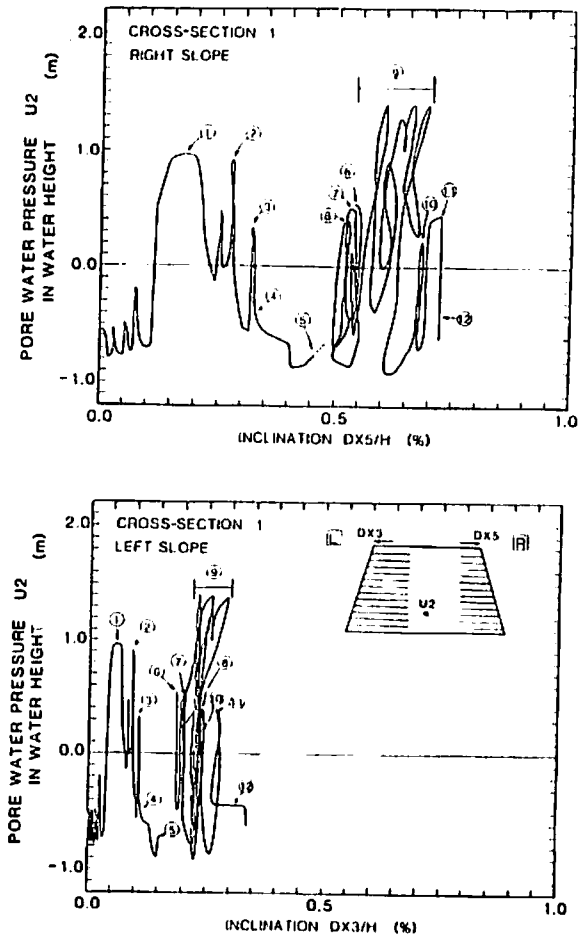

Fig. 10. Relationships between pore water pressure U2 and outward tilting of slopes; embankment II (see Fig. 4(b) for the legend of the numbers in circles).

U2 and U8 decreased and subsequently became positive. Figure 10 shows the relationships between the change in the pore-water pressure U2 and the outward tilting of both slopes. It may be seen that the behaviour resembles that of a visco-elasto-plastic material in the sense that (i) the deformation increases at a higher rate only when the pore-water pressure exceeds the previous maximum value and (ii) the creep deformation

continues, even at a virtually constant negative pore-water pressure, with the creep rate decreasing with time. In particular it may be seen that the incremental creep deformation in the second and following years was much less than that in the first year for both embankments I and II (see Figs 4–10). The explanation for this phenomenon may be as follows. Even for partly saturated soils it can be assumed that if the degree of saturation is high enough, as in this case, the shear strength of the soil is controlled by the effective stress (σ'), defined as $\sigma' = \sigma - u_w$, where σ is the total stress and u_w is the pore-water pressure.[4] Therefore the decrease in the negative pore-water pressures (suction), with the pore-water pressures subsequently becoming positive, means a decrease in the shear strength of soil. Since the soil was initially near full saturation in this case it is likely that the degree of saturation did not increase at a high rate even during heavy rainfall. Therefore the increase in the self-weight of soil during heavy rainfall can be ignored. Consequently the reduction in factor of safety against failure in soil can be attributed to a decrease in effective stress in soil and possible water pressure in vertical cracks. Some stresses in the soil may be transferred to the geotextile by the reduction in factor of safety against failure in soil. Then the outward horizontal displacement of the slopes takes place by the deformation of both the soil and the geotextile. It seems that, since the deformation characteristics of both the soil and the geotextile are visco-elasto-plastic, the overall deformation of the slopes shows a similar tendency.

(4) From the above it follows that preservation of a high soil suction is very important for maintaining slope stability, and the pore-water pressures within the embankment should be prevented from becoming positive, and water should be drained from vertical cracks (if any). It may be seen in Figs 4 and 5 that even during heavy rainfall the pore-water pressures in the soil layers between geotextile sheets (U1, U3, U4, U6 in cross-section 1; U7, U9, U10, U12 in cross-section 2) were still negative whereas the pore-water pressures in the unreinforced zones (U2, U5 in cross-section 1; U8 in cross-section 2) became positive. This behaviour clearly demonstrates that the non-woven geotextile functioned very effectively as a drainage material for these test embankments.

(5) The tensile strains in the geotextile were not measured for these two embankments. However, the following evidence shows that the non-woven geotextile did provide tensile reinforcement to the embankments. First of all, when embankment I was demolished major cracks were found only in the unreinforced zone between the right- and left-hand reinforced zones (Fig. 8). In the reinforced zones hair cracks were observed especially in the top soil layers and in the zones adjacent to the slope faces. It is to be noted that even in the left-hand slope, which experienced a large overall

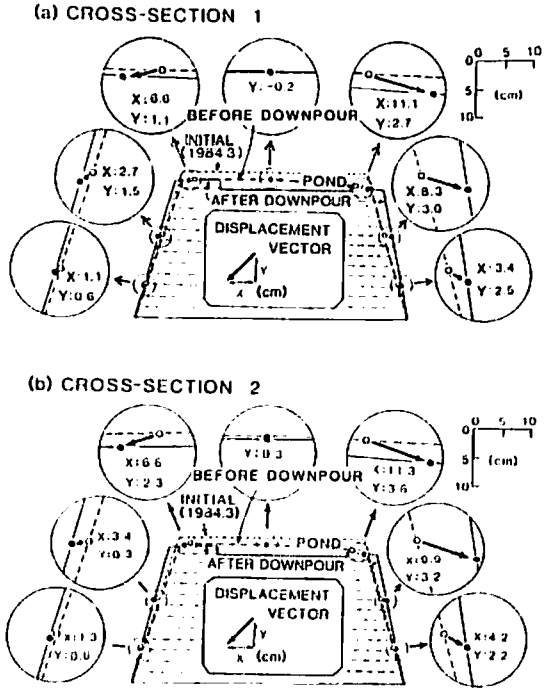

Fig. 11. Deformation of embankment II by artificial downpour in October 1985.

displacement, the reinforced zone overlying the lowest soil layer moved almost as a rigid body. Secondly, both slopes of embankment II rotated about their toes when a supply of about 70 m^3 of water was allowed to percolate through from its crest over a 2-week period in October 1985 (Fig. 11). It may be seen that the slope tilting was larger in the right-hand slope, which had shorter reinforcement, than in the left-hand slope which had longer reinforcement. Although several vertical cracks appeared in the unreinforced zone between the two reinforced zones, no clear cracks were observed in the crests of the reinforced zones. Apparently both slopes would have experienced failure in this artificial heavy downpour if these had not been reinforced. Lastly, another test embankment very similar to these two test embankments (A in Fig. 12) was constructed on a 7 m thick layer of a very soft fill of Kanto loam at another site in March 1985 by Nakamura *et al.*[5] The slope had a height of 3 m and a slope of 1:0·2 with the vertical spacing and the length of horizontal non-woven geotextile

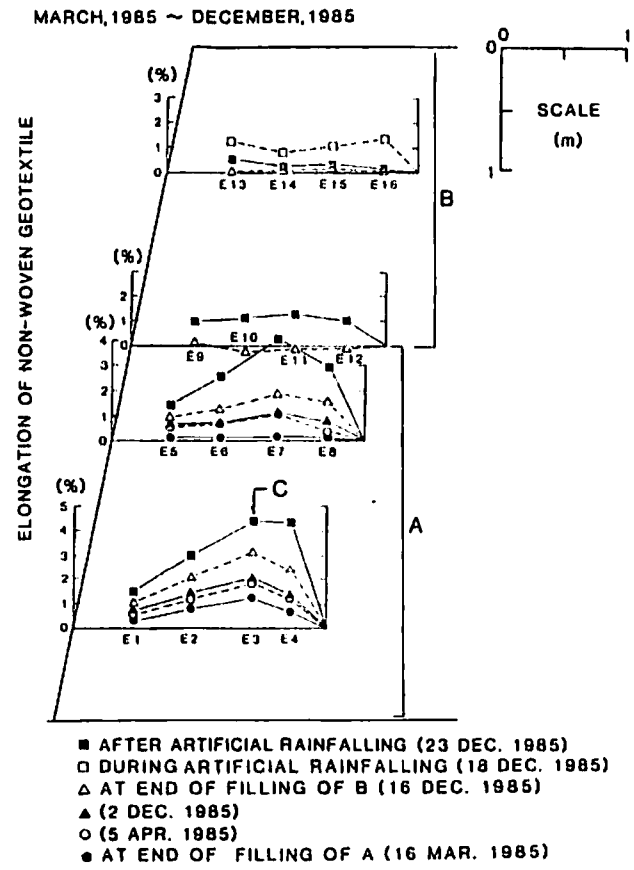

Fig. 12. Strain distribution of non-woven geotextile in a test embankment made by Nakamura *et al.*[5,6]

sheets being 0·5 m and 2 m respectively (Fig. 12). The slope face was covered with precast concrete facing panels connected to the geotextile sheets. Average tensile strains for a 0·5 m length in geotextile sheets were obtained from the elongation of the sheets measured by means of a newly developed method. This method will be described in a subsequent paper. In the geotextile layer at an elevation of 0·5 m the maximum tensile strain was observed 1·4 m behind the face and was about 1·2% at the end of filling. This strain increased to about 1·7% over the following 12 days and

increased to about 2% some 8 months after the end of filling. Then an additional reinforced soil layer, with a height of 2·4 m and a slope of 1:0·2 (B in Fig. 12), was placed above the existing slope in December 1985. This increased the strain to about 3%. The distributions of tensile strain seen in Fig. 11 seem to indicate that the non-woven geotextile sheets functioned as a tensile reinforcement. Then, under the effects of an artificial rainfall, equivalent to 620 mm of rain over 4 days, the slope experienced a considerable displacement although overall stability was maintained. It was again found, from demolishing the slope and observing the exposed cross-sections, that the major cracks were only in the unreinforced zone, showing that the reinforced zone displaced almost as a rigid body.

Generally, the creep elongation of non-woven geotextiles is larger than for other kinds of geotextiles. This behaviour may reduce long-term efficiency since relatively large deformations may occur in earth structures reinforced with a non-woven geotextile. However, the horizontal creep deformation of the two test embankments was found to be slight except in the first year as shown in Figs 4, 7 and 9. The explanation for this phenomenon may be that long-term sustained loads induced in the geotextile are smaller than those created when the effective stress in the soil is reduced and water pressure in vertical cracks is induced by heavy rainfall as illustrated schematically in Fig. 13. In fact, the creep strain rate of the non-woven geotextile at point C in the third test embankment (Fig. 12) decreased from about 3×10^{-3}%/day 1 week after the filling to

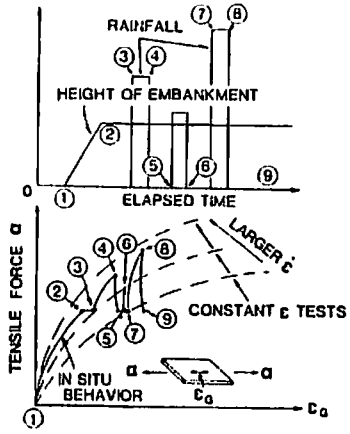

Fig. 13. Schematic diagram illustrating creep deformation of non-woven geotextile.

3×10^{-5}%/day 200 days after the filling.[6] Careful creep analyses are needed to explain this behaviour.

In summary, when a slight deformation of the embankment can be allowed, as is the case for many clay embankments, a non-woven geotextile soil reinforcement may be used. However, the combined use of a non-woven geotextile and a stiffer reinforcement such as polymer geogrid may be needed for critically high structures.

4 LABORATORY TESTS

When a material, such as a non-woven geotextile, having a relatively low Young's modulus is used as a tensile reinforcement its Poisson's ratio, when compressed normal to its plane, is also a very important factor. Figure 14 shows the stress regime and results of plane strain compression tests on either an unreinforced sand specimen or sand specimens reinforced with various materials listed in Table 3. Since stresses and strains within reinforced specimens are not uniform, $\bar{\sigma}_1$ is the *average* axial stress and $\bar{\varepsilon}_3$ is the *average* lateral strain which is taken to be negative. The deformation and strength properties of unreinforced Toyoura sand are given in detail elsewhere.[7]

Figure 15 shows the relationship between the reinforcing ratio defined as

$$R = \frac{[(\bar{\sigma}_1)_{max} \text{ for reinforced specimen}]}{[(\sigma_1)_{max} \text{ for unreinforced specimen}]} - 1{\cdot}0$$

and the tensile stiffness $E \cdot t$ where E is the Young's modulus and t is the thickness of the reinforcement. For the geotextile, the value of $E \cdot t$ is the secant modulus at an elongation of 15%, $\alpha_{0.15}/0{\cdot}15$ (Table 2). It may be seen that the measured reinforcing ratios are not a unique function of $E \cdot t$, but they are larger for the geotextile than for rubber ($\nu \doteqdot 0{\cdot}5$) at the same value of $E \cdot t$. On the other hand, when the stress non-uniformity in the reinforced soil is ignored and when the increase in the average confining pressure is represented by $\Delta\sigma_3$, the reinforcing ratio is given by

$$R = \frac{(\sigma_{3_0} + \Delta\sigma_3) K_p}{\sigma_{3_0} K_p} - 1 = \frac{\Delta\sigma_3}{\sigma_{3_0}} \tag{2}$$

where σ_{3_0} is the confining pressure which is equal to 49 kN/m^2 for the data shown in Fig. 14 and $K_p = (1 + \sin\varphi)/(1 - \sin\varphi)$ where φ is the angle of internal friction of the test sand. The assumption above as to the stress uniformity becomes less accurate for stiffer reinforcements. Then the

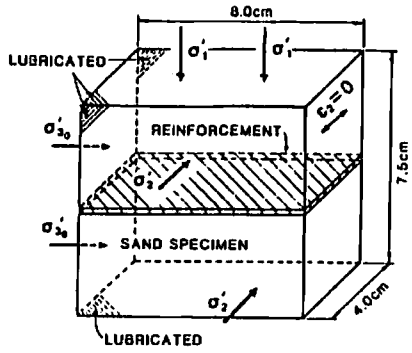

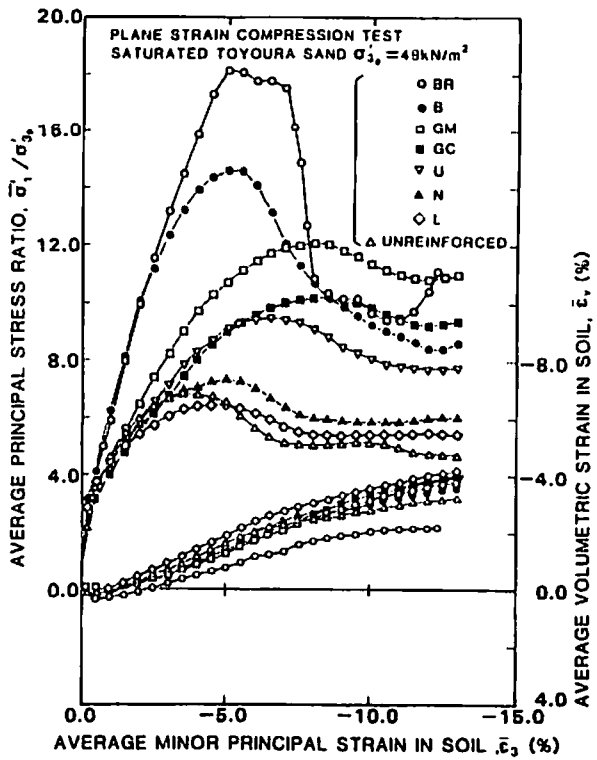

Fig. 14. Plane strain compression test results for unreinforced and reinforced sand specimens.

TABLE 3
Physical Properties of Reinforcements used for Plane Strain Compression Tests

Symbol	Reinforcement	Young's modulus, E (kN/m^2)	Poisson's ratio, ν	$\frac{(1+\nu)\nu}{E}$ (m^2/N)	Thickness (mm)	Friction angle against Toyoura sand
BR	Very rough[a] brass plate	$1{\cdot}01 \times 10^5$	—	0	0·5[e] (1·6)[f]	$>\phi$[h]
B	Brass plate	$1{\cdot}01 \times 10^8$	—	0	0·5	21[c]
GM	Non-woven geotextile (machine direction)	1×10^4 to $1{\cdot}4 \times 10^4$[g]	0·0	0	$t_0 \doteqdot 4$[b]	$>\phi$[d]
GC	Non-woven geotextile (cross directions)	2×10^3 to 8×10^3[g]	0·0	0	$t_0 \doteqdot 4$[b]	$>\phi$[d]
U	Urethane	$4{\cdot}51 \times 10^4$	0·5	0·016	1·0	$>\phi$
N	Neoprene	$2{\cdot}70 \times 10^4$	0·5	0·028	1·0	$>\phi$
L	Latex	$1{\cdot}47 \times 10^3$	0·5	0·51	2·32	$>\phi$

[a] Roughened by gluing Toyoura sand particles to its surfaces.
[b] Unstressed thickness.
[c] Measured at a normal stress of 98 kN/m^2.
[d] Measured by direct shear tests.[7]
[e] Thickness excluding glued sand particles.
[f] Thickness including glued sand particles.
[g] Values at an elongation of 15% (see Table 2). $E = (\alpha_{0\cdot15}/0\cdot15)$/(thickness when compressed).
[h] ϕ: angle of internal friction of Toyoura sand.[7]

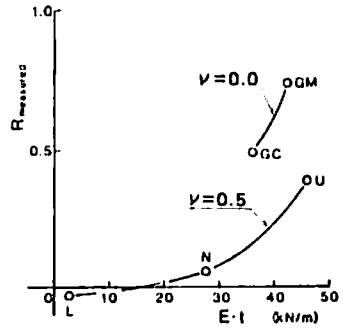

Fig. 15. Relationship between reinforcing ratio R and $E \cdot t$ in plane strain compression tests.

average tensile force per width working in the reinforcement T at failure is given as

$$T = \Delta\sigma_3 \times \Delta H = (\bar{\epsilon}_{xR} - \bar{\epsilon}_{3R}) \times E \cdot t \tag{3}$$

where ΔH is the vertical spacing between the reinforcements, which is the height of specimen in this case, $\bar{\epsilon}_{3R}$ is the lateral strain (negative) at failure in the unreinforced soil specimen confined by $(\sigma_{3_0} + \Delta\sigma_3)$ and $\bar{\epsilon}_{xR}$ is the lateral strain (negative) at failure in the reinforcement when this alone is compressed by the axial stress of $(\sigma_{3_0} + \Delta\sigma_3)K_p$ from the isotropic stress condition at the confining stress of σ_{3_0}. The value of $\bar{\epsilon}_{xR}$ is obtained by using the plane strain condition $\epsilon_2 = 0$ as

$$\bar{\epsilon}_{xR} = -\frac{(1+\nu)\nu}{E}[(K_p - 1)\sigma_{3_0} + K_p\Delta\sigma_3] \tag{4}$$

By substituting eqns (3) and (4) into eqn (2) we obtain

$$R = \left[-\frac{\bar{\epsilon}_{3R}}{\sigma_{3_0}} - \frac{(1+\nu)\nu}{E}(K_p - 1)\right] \Big/ \left[\frac{\Delta H}{E \cdot t} + \frac{(1+\nu)\nu}{E}K_p\right] \tag{5}$$

Measured and theoretical eqn (5) values of R are compared in Fig. 16. It may be seen from Fig. 16 that eqn (5) models the test results well despite simplifying assumptions made in deriving it.

A similar result was also obtained from model bearing capacity tests of a strip footing on sand (Fig. 17). The sand box had a width of 40 cm with well-lubricated side surfaces. It may be seen that a sheet of the non-woven geotextile having the same width as the model footing improved the

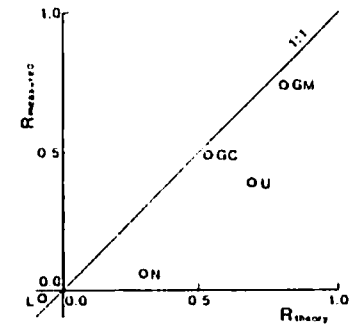

Fig. 16. Relationship between measured and theoretical values of R.

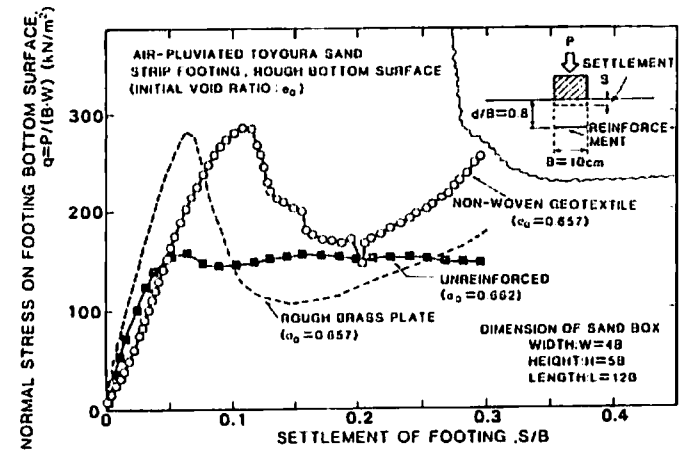

Fig. 17. Model bearing capacity test results for reinforced and unreinforced sand grounds.

bearing capacity to a similar extent as a rough brass plate whereas the compressibility of the ground was increased because of a larger compressibility of the non-woven geotextile.

These laboratory test results seem to indicate that the non-woven geotextile can perform as a tensile soil reinforcement. However, a larger soil deformation is needed to mobilize a sufficient degree of tensile restraint in the non-woven geotextiles than might be expected for stiffer reinforcing materials.

5 STABILITY ANALYSIS

The overall stability of the horizontal force of the slopes of embankment II was examined using a limit equilibrium method. This was based on a two-part wedge failure mechanism proposed by Jewell *et al.*[8] (Fig. 18). In the analyses a soil–geotextile friction angle (φ_μ) of 30° and the tensile strength of the geotextile (σ_t) given in Table 2 were used. The soil friction along the surface bd in Fig. 18 was ignored. The active earth pressure was

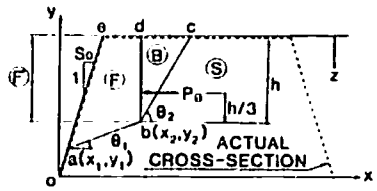

Fig. 18. Two-part wedge failure mechanism.[8]

assumed along the slope height since the non-woven geotextile is rather extensible. The earth pressure (P_B) is assumed to be the Rankine active earth pressure with $\theta_2 = 45° + \varphi'/2$. The gross required tensile reinforcement force (T_{req}) is defined as the additional horizontal force required for the static equilibrium in an unreinforced slope for the assumed failure mechanism; therefore T_{req} is a function of the coordinates of the points a,b and the angle θ_1. The gross tensile reinforcement force (T_{avail}) available for the assumed failure mechanism is given by

$$T_{avail} = \sum (T_{avail})_i$$

$$(T_{avail})_i = \min[(R_T)_i, (T_A)_i] \tag{6}$$

where $(T_{avail})_i$ is the tensile force available for each layer of reinforcement, $(R_T)_i$ is the tensile strength of the reinforcement in the ith layer and $(T_A)_i$ is the pull-out resistance for the reinforcement in the ith layer having a length $(L_A)_i$ extending behind the failure surfaces ab and bc, which is given by $(T_A)_i = 2\gamma_t z_i \tan\varphi_\mu (L_A)_i$. A soil unit weight $\gamma_t = 1{\cdot}34$ tf/m^3 (13·1 kN/m^3) was used. The safety factor is defined as SF = $\min(T_{avail}/T_{req})$ for all possible failure mechanisms.

Furthermore, the effect of rainfall was taken into account as a reduction of the negative pore water pressure (suction), but positive pore water pressure was not considered. The water pressure in possible vertical cracks was also ignored. The effect of positive pore water pressure and water

pressure in vertical cracks should be taken into account when these cannot be ignored. Therefore the shear strength of the soil was given by

$$\tau_f = (\sigma - u_w)\tan\varphi' \tag{7}$$

where σ is the total normal stress and u_w is the pore water pressure. For $\varphi' = 30°$ and $u_w = 0$, the values of SF were 1·41 for the right-hand slope and 3·36 for the left-hand slope of embankment II for the failure mechanisms indicated in the insets in Fig. 19 (a) and (b). The strength parameters in effective stress $\varphi' = 30°$ and $c' = 0$ were selected based on the results of undrained triaxial compression tests with the pore water pressure measurement on samples reconstituted from the slurry of Kanto loam taken from the site. Therefore these strength parameters can be considered to be a lower bound for the soil of the embankments. The effect of the reinforcement length can be seen in the results. These results also indicate that for the right-hand slope the local stability of both the lowest sheet of geotextile and the lowest two soil layers, which are designated A in Fig. 19(a), is very important regarding the overall stability of the slope. It is to be noted that when the slope facing has not sufficient ability to confine the soil near the slope toe, which is designated B in Fig. 19(a), large local compression in the soil may occur which can trigger the overall instability of the slope. This was in fact the case for the left-hand slope of embankment I. Figure 19 (a) and (b) also shows the change of the ratio T_{avail}/T_{req} by the change of the vertical coordinate y_2 for the fixed coordinate x_2. It may be seen that the ratio T_{avail}/T_{req} is not the minimum for the mechanism where T_{req} becomes the maximum. This result indicates that it is not sufficient to examine the stability for the failure mechanism of the unreinforced slope concerned.

Figure 20(a) shows the relationship between safety factor and u_w (negative) for the right-hand slope of embankment II. It may be seen that the effect of negative pore water on the overall stability of the slope is significant. The safety factor increases remarkably from 1·41 to 13·06 when u_w changes from zero to only a −0·9 m head of water. This significant increase in safety factor with increase in magnitude of $-u_w$ is due to the increase in the critical angle θ_1 associated with the increase in $-u_w$. T_{avail} increases rapidly with increase in θ_1, and while T_{req} increases at a small rate at small θ_1 it decreases at larger values of θ_1. This result clearly indicates the importance of the ability of the reinforcement to drain such clay slopes. Figure 20(b) shows the relationship between safety factor and the angle of internal friction (φ') for $u_w = 0$. This result indicates that to increase φ' of the soil by better compaction is an effective measure. However, it is to be noted that the increase in φ' from 30° to 40°, when $u_w = 0$, is equivalent to a decrease in u_w from 0 to about a −0·6 m head of water when $\varphi = 30°$.

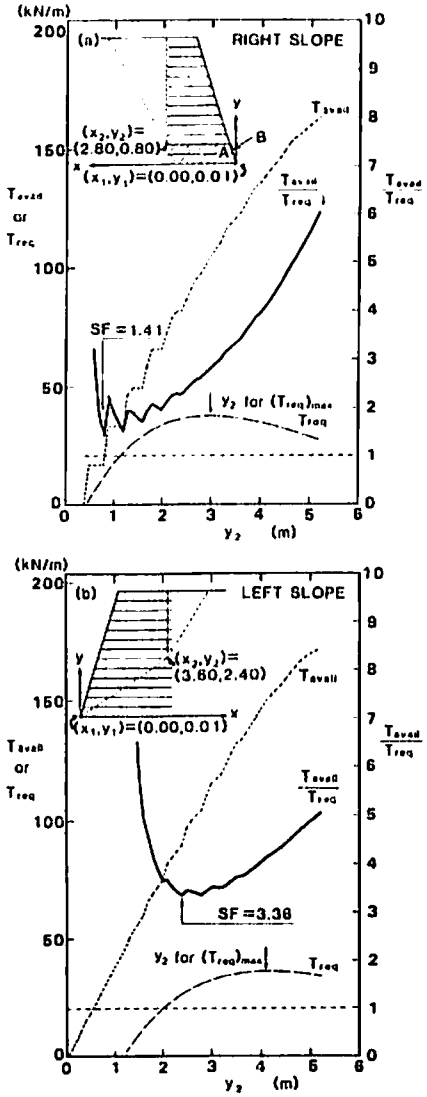

Fig. 19. Results of stability analyses for embankment II.

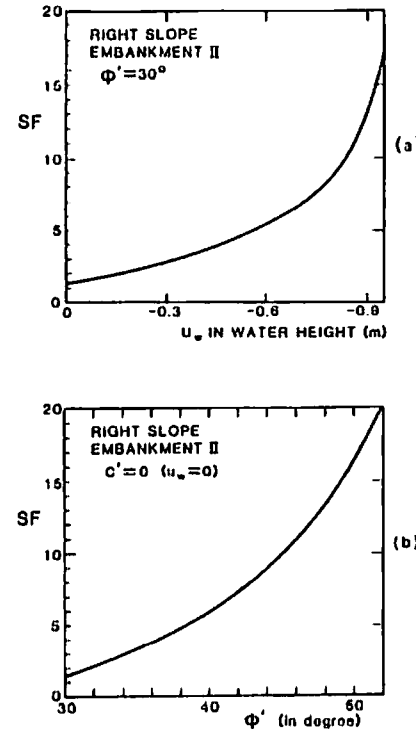

Fig. 20. Effects of (a) suction $-U_w$ and (b) φ' on the factor of safety (SF) for the right-hand slope; embankment II.

The analytical results presented herein are not the final ones. In particular, much more accurate evaluations of strength parameters of soil are needed and the stability analyses for the overturning about the slope toe are also required for slopes reinforced with a short geotextile. The final evaluation will be conducted after laboratory tests of soil strengths on samples taken from the interior of these test embankments.

6 CONCLUSIONS

Two test embankments of volcanic ash clay reinforced with a non-woven geotextile were constructed. It was found that non-woven geotextile sheets are very useful for allowing better compaction, draining pore water from the interior of embankments and tensile soil reinforcement. It was found

that, to achieve a performance of reinforced slopes within acceptable tolerances, the vertical spacing of the geotextile sheets should not be too large, the length of the geotextile sheets should not be too small, and some measures are needed to confine soil layers near the slope surfaces. The performance of the two test embankments was partly explained by laboratory loading tests (on reinforced plane strain samples), model tests and stability analyses using a limit equilibrium method in terms of effective stresses.

ACKNOWLEDGEMENTS

The authors wish to thank Mr K. Iwasaki of Mitsui Petrochemical Industries Ltd., Mr K. Nakamura and Mr Y. Tamura of Tokyu Construction Co., Mr S. Yamamoto and Mr H. Kuwabara of Tokyo Electronic Power Co., and Mr T. Sato, Mr S. Yamada and Mr T. B. S. Pradhan of the University of Tokyo for their co-operation in this study. The assistance of Miss M. Torimitsu in preparing the manuscript is also appreciated. This study was partly sponsored by the Ministry of Education of the Japanese Government.

REFERENCES

1. Ingold, T. S. and Templeman, L. E., The comparative performance of polymer net reinforcement. *Proc. Int. Conf. on Use of Fabrics in Geotechniques*, Paris, 1 (1977) 65–70.
2. Tatsuoka, F., Ando(Yamauchi), H., Iwasaki, K. and Nakamura, K., Performances of clay test embankments reinforced with a non-woven geotextile. *Proc. 3rd Int. Conf. Geotextiles*, Wien (1986).
3. Andrawes, K. Z., McGown, A. and Kabir, M. H., Uniaxial strength testing of woven and nonwoven geotextiles. *Geotextiles and Geomembranes*, 1 (1984) 41–56.
4. Bishop, A. W. and Blight, G. E., Some aspects of effective stress in saturated and partly saturated soils. *Géotechnique*, 13 (1963) 177–97.
5. Nakamura, K., Kuroda, E., Tamura, Y. and Iwasaki, K., Slope reinforcing by means of non-woven fabric (Part 3), *Proc. Jap. Ann. Symp. SMFE* (1986).
6. Tamura, Y., Nakamura, K., Mashiko, T., Minami, T. and Yamauchi, H., Slope reinforcing by means of non-woven fabric (Part 1), *Proc. Jap. Ann. Symp. SMFE* (1986).
7. Tatsuoka, F., Sakamoto, M., Kawamura, T. and Fukushima, S., Strength and deformation characteristics of sand in plane strain compression at extremely low pressures. *Soils and Foundations*, 26 (No. 1) 65–84.
8. Jewell, R. A., Paine, N. and Woods, R. I., Design methods for steep reinforced embankments, *Proc. Symp. Polymer Grid Reinforcement in Civil Engng*, London (1984) Paper No. 31.

Geotextiles and Geomembranes 4 (1986) 269–284

Comparative Studies of Design and Construction of a Steep Reinforced Embankment

N. Fukuda

Fukken Co. Ltd., 2-10-11 Hikari-cho Higashi-ku Hiroshima, 732, Japan

T. Yamanouchi

Faculty of Engineering, Kyushu Sangyo University, Matsukadai, Fukuoka, 813, Japan

and

N. Miura

Faculty of Science and Engineering, Saga University, Saga, 840, Japan

ABSTRACT

The design of steep reinforced embankments using high tensile polymer grids has to be formulated making several assumptions. The present paper deals with laboratory tests and instrumented embankments constructed to investigate the validity of the assumptions made. Laboratory tests were conducted using a soil container with one layer of grid. Test results obtained from two kinds of grid condition were found to be in agreement with the proposed design method based on 'tie-back-wedge-analysis'. A vertical faced embankment and an embankment with a sloping face were constructed using horizontal layers of grid reinforcement. Measurements of the tensions in the grids were found to be considerably less than those predicted by the design method. These studies reveal that the reinforcing effect is greater than that assumed in the design since the fill material is integrated with polymer grids laid in the embankment. It is suggested that such an integration effect should be incorporated in future design methods.

1 INTRODUCTION

High tensile strength geotextiles are particularly applicable as reinforcing materials for steep embankments and earth retaining structures. These

Geotextiles and Geomembranes 0266-1144/86/$03·50